Received: 16 December 2019 | Revised: 4 May 2020 | Accepted: 5 May 2020

DOI: 10.1111/jace.17215

Journal of the American Ceramic Society

ORIGINAL ARTICLE

The effect of microencapsulated phase change materials on the rheology of geopolymer and Portland cement mortars

Shima Pilehvar[1] | **Anna M. Szczotok**[1] | **Manuel Carmona**[2] | **Ramón Pamies**[3] | **Anna-Lena Kjøniksen**[1]

[1]Faculty of Engineering, Østfold University College, Halden, Norway

[2]Department of Chemical Engineering, University of Castilla – La Mancha, Ciudad Real, Spain

[3]Departamento de Ingeniería Mecánica, Materiales y Fabricación, Universidad Politécnica de Cartagena, Cartagena, Spain

Correspondence
Anna-Lena Kjøniksen, Faculty of Engineering, Østfold University College, P.O. Box 700, 1757 Halden, Norway.
Email: anna.l.kjoniksen@hiof.no

Funding information
Norges Forskningsråd, Grant/Award Number: 238198; Fundación Séneca Agencia de Ciencia y Tecnología de la Región de Murcia, Grant/Award Number: 19877/GERM/14

Abstract

The effect of microencapsulated phase-change materials (MPCM) on the rheological properties of pre-set geopolymer and Portland cement mortars was examined. Microcapsules with hydrophilic and hydrophobic shells were compared. The shear rate dependency of the viscosities fitted well to a double Carreau model. The zero shear viscosities are higher for geopolymer mortar, illustrating poorer workability. The time evolution of the viscosities was explored at shear rates of 1 and 10 s^{-1}. New empirical equations were developed to quantify the time-dependent viscosity changes. The highest shear rate disrupted the buildup of the mortar structures much more than the lower shear rate. Microcapsules with a hydrophobic shell affect the rheological properties much less than the microcapsules with a hydrophilic shell, due to the higher water adsorption onto the hydrophilic microcapsules. Shear forces was found to break down the initial structures within geopolymer mortars more easily than for Portland cement mortars, while the geopolymer reaction products are able to withstand shear forces better than Portland cement hydration products. Initially, the viscosity of geopolymer mortars increases relatively slowly during due to formation of geopolymer precursors; at longer times, there is a steeper viscosity rise caused by the development of a 3D-geopolymer network. Disruption of agglomerates causes the viscosities of portland cement mortars to decrease during the first few minutes, after which the hydration process (increasing viscosities) competes with shear-induced disruption of the structures (decreasing viscosities), resulting in a complex viscosity behavior.

KEYWORDS

geopolymer, phase change materials, Portland cement, rheology

1 | INTRODUCTION

Geopolymers are synthesized by reaction of amorphous aluminosilicates, for example, fly ash or slag, with a concentrated alkaline solution such as sodium hydroxide or sodium silicate.[1] Geopolymers have a high potential as substitutes for Portland cement due to better performance and an environmentally friendly profile.[2]

Phase change materials (PCMs) are very useful for thermal energy storage. When the temperature is higher than melting point of the PCM, the excess heat is absorbed by melting the PCM. When the temperature decreases, the heat is released into the environment by solidifying the PCM.[3] There are, however, several disadvantages to utilizing bulk quantities of PCMs, such as low thermal conductivity, solidification only around the edges, and reduced heat transfer.[4,5] By encapsulating the PCM in microcapsules, it is possible to prevent both leakage of the PCM and interaction between the PCM and building materials. In addition, microencapsulation improves the heat transfer area, and the microcapsules can withstand volume change during phase change.[6] Microencapsulated phase change materials (MPCMs) therefore provide an efficient method for storing thermal energy, utilizing the relatively large surface area and high latent heat. Incorporation of MPCMs into building materials, such as mortar and concrete, can improve the energy storage capacity and thereby reduce indoor temperature fluctuations and save energy.[7,8,9,10] Previous results illustrate that the MPCMs utilized in the current study are efficient for reducing the energy needed to keep a comfortable indoor temperature.[9,10,11,12,13]

Unfortunately, there is a decline in the compressive strength of concrete with the addition of MPCM.[12,14,15,16,17] This is reported to be a combination of several factors: (a) the MPCM particles are softer than to the other solids in the mixture,[16,17] (b) the addition of MPCM causes more air voids to be formed within the matrix,[12,14] and (c) air gaps is formed between MPCM and the surrounding matrix.[14,15] In addition, the workability of concrete becomes poorer with the addition of MPCM due to water adsorbing onto the microcapsules, which decreases the available water in the samples and causes lower slump values.[15,18]

Rheological characterization is required to examine the early age properties of building materials such as workability, consistency, and flow behavior, which are important for casting and molding.[19] There are several studies regarding the rheological behavior of geopolymer and Portland cement mixtures combined with small particles such as nanosilica,[20,21,22] nanoclays,[21,23] limestone,[24] graphene oxide,[25,26] carbon nanotubes,[27] rubbers,[28,29] as well as various fibers[30,31,32] and aggregates.[33] The overall picture is that adding small particles to geopolymer or Portland cement mixtures affect the rheological properties in different ways, depending on the size, shape, and surface properties of the particles, as well as whether they interact physically or chemically with any of the other components in the composite.

There are very few studies examining how the rheology of geopolymers or Portland cement composites is affected by MPCM addition.[15,18,34,35,36] Most previous studies only measure slump, which generally show that MPCM addition increase the water demand to obtain a constant slump value,[34,36] or analogously that adding microcapsules decrease the slump.[15,18,36] More thorough rheological investigations utilizing rheometers or viscosimeters are scarce.[35,36] Shear rate dependencies of Portland cement paste containing MPCM has been examined, and it was found that the pastes went from shear thinning to shear thickening behavior when the amount of superplasticizer was increased.[36] The time-dependent viscosities of geopolymer pastes containing three different MPCMs have been studied at a constant shear rate.[35] It was found that at the start of the reaction, there was a slow viscosity increase due to the formation of geopolymer precursors, and that these precursors formed faster in the presence of MPCM. At longer times, there was a steeper viscosity increase due to geopolymer formation, which was slowed down with MPCM addition. There are, however, no previous studies of shear rate dependencies or the time development of viscosities of either Portland cement mortars (PMs) of geopolymer mortars (GMs).

The non-Newtonian rheological behavior of fresh constructing materials has been studied in the past decades.[37] However, the description of the flow behavior by current models does not address the time dependence of these materials.[38] There is a lack of models describing the time dependency of the viscosities of mortars that exhibit complex viscosity changes. In addition, few experimental studies have explored this problem.[39]

It is therefore interesting to investigate how the MPCM can affect the viscosity of mortars. Since different types of MPCM may not have the same influence on the viscosity, two kinds of MPCMs with hydrophobic and hydrophilic shells were compared. In addition, the MPCM concentration was varied (replacing 0-20 vol% of the sand). Both the shear rate dependency of the viscosities of mortars shortly after mixing and the development of the viscosities over time has been explored. A double Carreau model has been used to describe the shear rate dependency of the viscosities. New empirical equations have been developed to quantify the time-dependent changes of the viscosities and the reaction kinetics.

2 | EXPERIMENTAL PROCEDURE

2.1 | Materials

The materials used in GM were class F fly ash (density = 2.26 ± 0.02 g/cm^3) and ground granulated blast furnace slag (density = 2.85 ± 0.02 g/cm^3) as geopolymer binder, sodium hydroxide pellets (density = 2.13 g/cm^3) and sodium silicate solution (density = 1.93 g/cm^3, 35 wt% solid) as the alkaline solution. The composition of the fly

TABLE 1 Mix design of geopolymer mortar

MPCM (vol%)	Alkaline solution (g)	Fly ash (g)	Slag (g)	Extra water (g)	Sand (g)	MPCM (g)
0	72.68	109	72.68	27.25	316.56	0
5	72.68	109	72.68	27.25	300.73	5.48
10	72.68	109	72.68	27.25	284.91	10.96
15	72.68	109	72.68	27.25	269.08	16.43
20	72.68	109	72.68	27.25	253.25	21.92

Note: The MPCM percentages indicate the volume of sand replaced by MPCM

TABLE 2 Mix design of portland cement mortar

MPCM (vol%)	Cement (g)	Water (g)	Sand (g)	MPCM (g)
0	181.68	87.21	331.13	0
5	181.68	87.21	314.58	5.73
10	181.68	87.21	298.02	11.46
15	181.68	87.21	281.47	17.19
20	181.68	87.21	264.91	22.92

Note: The MPCM percentages indicate the volume of sand replaced by MPCM.

ash class F (FA) is 50.83 wt% SiO_2, 23.15 wt% Al_2O_3, and 6.873 wt% CaO. The ground granulated blast furnace slag (GGBFS) consists of 34.51 wt% SiO_2, 10.3 wt% Al_2O_3, and 42.84 wt% CaO. For the preparation of PM, Portland cement II mixed with FA (density = 3.0 g/cm^3) was utilized. The main components of the Portland cement/fly ash mixture are 53.9 wt% CaO, 21.9 wt% SiO_2, 6.7 wt% Al_2O_3, 5.2 wt% Fe_2O_3, 4.2 wt% SO_3, 2.6 wt % CO_2, 1.5 wt% MgO, and 1.2 wt % K_2O. The same CEN-Standard sand EN 196-1 (density = 2.6 g/cm^3) was used for GM and PM. Two chemical admixtures, FLUBE OS 39 (density of 1.20 g/cm^3) and Dynamon SR-N (density of 1.1 g/cm^3) were used for GMs and PMs, respectively.

Two different MPCMs were utilized. Both PE-EVA-PCM and St-DVB-PCM are composed of a paraffin Rubitherm®RT27 core coated with a copolymer shell. PE-EVA-PCM has a relatively hydrophilic shell consisting of low-density polyethylene (LDPE) and ethylvinylacetate (EVA).[40] The hydrophobic shell of St-DVB-PCM contains styrene (St) and divinylbenzene (DVB).[6] PE-EVA-PCM and St-DVB-PCM have been found to adsorb 1.75 and 0.7 grams of water per mL MCPCM, respectively.[18]

2.2 | Size distributions

The particle size distribution of FA, GGBFS, cement, and MPCMs were determined by low angle laser light scattering laser diffraction (Malvern Mastersizer 2000). The size distribution of the sand was provided by the manufacturer.

2.3 | Mixing methods

For GMs, an alkaline solution with a sodium silicate solution to sodium hydroxide solution (14 mol/L) ratio of 1.5 was prepared 1 day in advance to ensure complete dissolution of NaOH pellets and to lose the exothermic reaction heat.

To achieve the same initial workability and fluidity of GMs and PMs, a flow table machine was used to determine the ratio of alkaline solution to geopolymer solids and water to cement (w/c) for GMs and PMs mix designs, respectively. In order to gain a better consistency for both mortars, a low dosage (1 wt% of binder) of two different chemical admixtures (FLUBE OS 39 and Dynamon SR-N) were utilized. The required amounts of MPCM in mortar mixtures were determined by its volume percentage and replaced a certain percentage of the sand.

For GMs, geopolymer binder (fly ash + slag), alkaline solution, and extra water were mixed together for 1 minute. After 30 seconds resting, sand, MPCMs, and chemical admixture were added and mixed for 2 minutes to achieve a homogeneous mortar. For PMs, cement, sand, and water were mixed for 1 minute. After 30 seconds resting, MPCMs and chemical admixture were introduced, and mixing was continued for 2 minutes. Accordingly, for GM without MPCMs, a total amount of liquid (alkaline solution + extra water) to geopolymer binder ratio of 0.55 was selected whereas a w/c ratio of 0.48 was chosen for PM without MPCMs. The mix designs of GMs and PMs are shown in Tables 1 and 2, respectively.

2.4 | Characterization of microcapsules

Figure 1 shows images and Figure 2 particle size distributions of the solid components of mortars, to illustrate the differences in shape and size. While St-DVB-PCM have a spherical shape (Figure 1B), PE-EVA-PCM exhibits a more uneven structure (Figure 1A). In addition, St-DVB-PCM is somewhat smaller and seems to have a narrower size distribution than PE-EVA-PCM (Figure 2). The sand is nonspherical (Figure 1C,D) and much larger than the microcapsules (Figure 2). Accordingly, replacing some of the sand with microcapsules results in a sample with a smaller size distribution. The slag, fly ash, and Portland cement have quite wide size distributions, where most

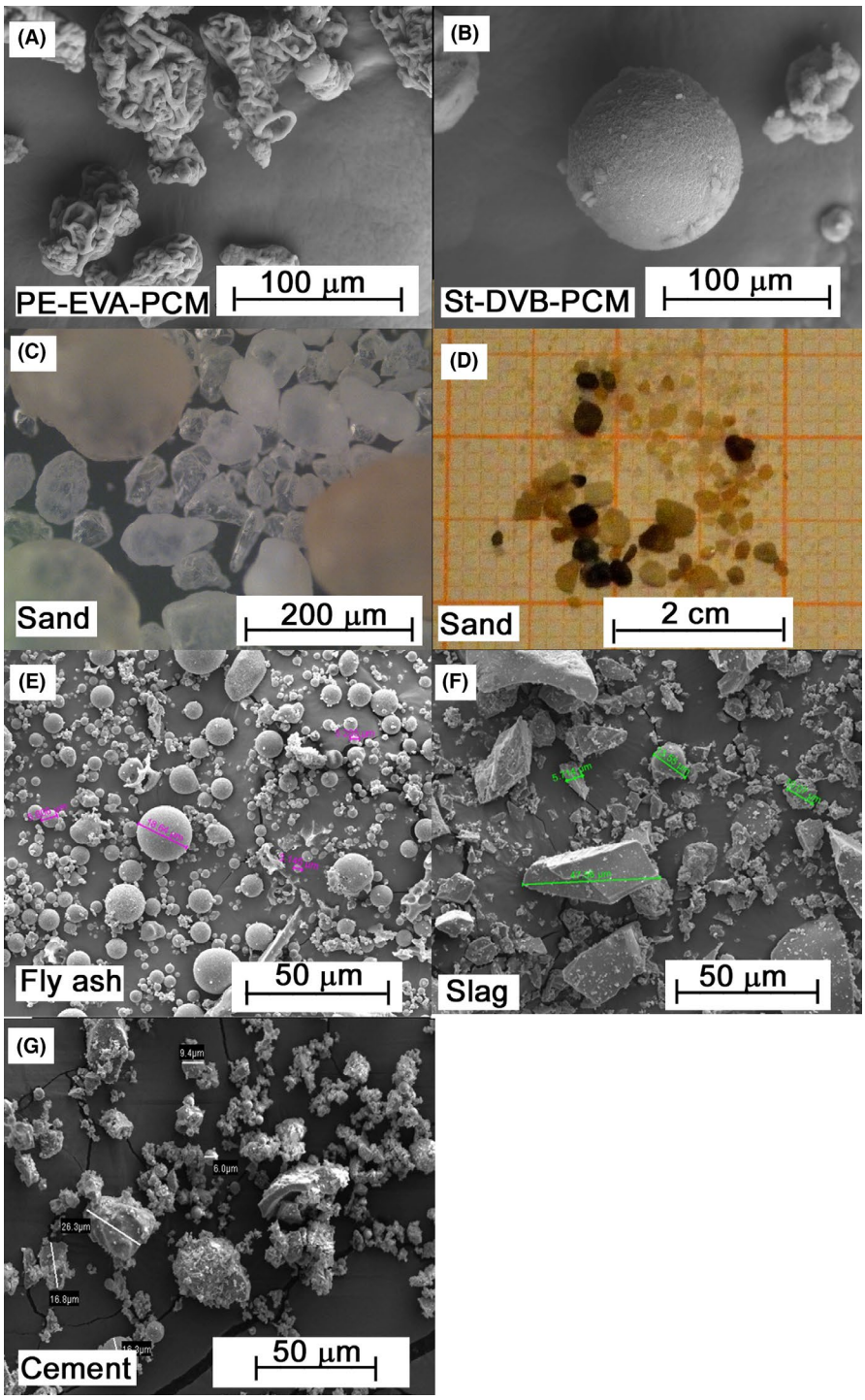

FIGURE 1 A, SEM image of PE-EVA-PCM, (B) SEM image of St-DVB-PCM, (C) microscope image of the sand, (D) picture of the sand (the mm-paper in the background provides a size reference), (E) SEM image of fly ash, (F) SEM image of slag, (G) SEM image of Portland cement

of the particles are smaller than the microcapsules (Figure 2). Fly ash particles are mostly spherical (Figure 1E), while the slag has an irregular shape with sharp edges (Figure 1F); Portland cement has an uneven shape (Figure 1G).

2.5 | Rheological measurements

Rheological measurements were carried out using an Anton Paar MCR302 rheometer (Austria) at 20.0°C. The samples were tested using a BMC-90 (building materials cell) measuring system (cup diameter: 74 mm; stirrer ST59-2V-44.3/120, diameter: 59 mm) mounted in a cylindrical Peltier system for temperature control. As illustrated in Figure 3, the cylinder walls are specially designed to avoid slippage, and the stirrer is designed for these kinds of building materials. After mixing, the mixture was loaded into the rheometer measuring cell. Great care was taken to ensure that the measurements of all samples were conducted at the same time after initiating the mixing of the components. The sample was first

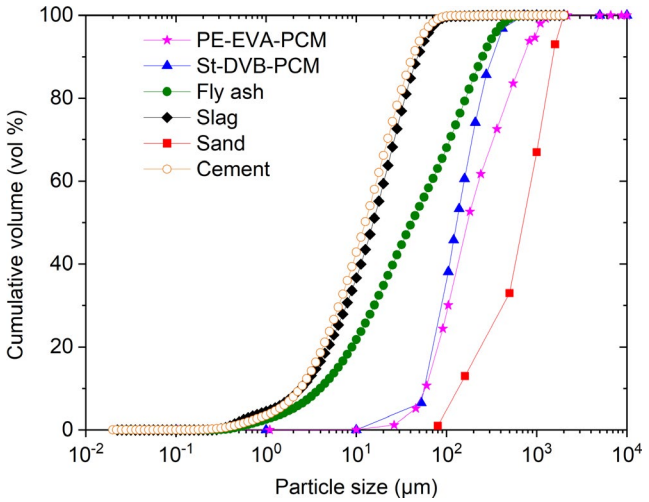

FIGURE 2 Particle size distributions of the solid components

FIGURE 3 Measuring system for the rheological experiments

left in the cell for 1 minute at a shear of 1 s^{-1}. After this, a pre-shear of 50 s^{-1} was applied for 30 seconds, followed by 1 s^{-1} for 30 seconds to ensure that the samples have the same the shear history. The high accuracy of the rheometer allows measurements even at very low shear rates. For the shear rate–dependent measurements, the samples were therefore measured from 10^{-4} s^{-1} to 100 s^{-1} using a logarithmic ramp with 1 second per data point and 61 data points. Since the reactions continue during the measurements, the total time of the shear rate sweep was kept at only 61 seconds to minimize any reaction-induced changes to the samples during measurements. For the time-dependent measurements, the samples were measured at a constant shear rate of 1 s^{-1} or 10 s^{-1} with 1 second per data point for 2000 seconds or until the samples became too viscous for measurements.

2.6 | Analysis of shear rate dependent viscosities

Several models have been used to describe non-Newtonian behavior.[41,42,43,44,45] For construction materials, models such as Power law (Ostwald-deWaele),[36,44,45] Bingham and modified Bingham,[43,44,45,46,47] Herschel-Bulkley,[43,44,45,47] Casson,[43,44,45,47] Sisko,[43,45,46] De Kee,[43,44,47] and Carreau[45,48,49] (and many more) have been utilized. The Carreau model[50] has previously been shown to give the best prediction of non-Newtonian fluids of suspended solids.[42] However, the mortars examined in the current study reveal a more complex behavior. As seen in Figure 4, the samples have a Newtonian plateau at low shear rates followed by a shear thinning region. At intermediate shear rates, there is a new plateau before a new shear thinning region is observed at high shear rates. Since the experimental data cannot be fitted by a single Carreau model, the shear rate ($\dot{\gamma}$)–dependent viscosities (η) are fitted to a sum of two Carreau models:

$$\eta(\dot{\gamma}) = (\eta_0 - \eta_p)\left[1 + \left(\frac{\dot{\gamma}}{\dot{\gamma}_1}\right)^2\right]^{\frac{n_1-1}{2}} + (\eta_p - \eta_\infty)\left[1 + \left(\frac{\dot{\gamma}}{\dot{\gamma}_2}\right)^2\right]^{\frac{n_2-1}{2}} + \eta_\infty \quad (1)$$

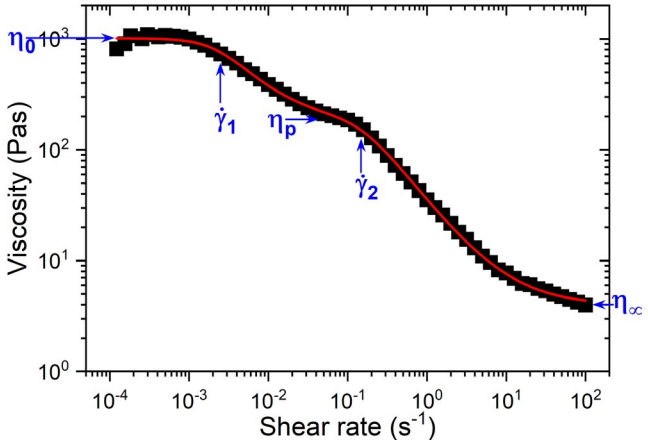

FIGURE 4 Example of the shear rate dependent viscosities. The symbols are the measured data, and the line is fitted by Equation 1. Some of the fitted parameters are illustrated in the figure

where η_0 is the zero shear viscosity, η_p is the viscosity at the plateau region at intermediate shear rates, η_∞ is the viscosity at infinite shear rates, $\dot{\gamma}_1$ and $\dot{\gamma}_2$ are, respectively, the shear rates where the first and second shear thinning regions starts, and n_1 and n_2 are the flow behavior indexes of the first and second shear thinning regions, respectively. Some of the fitted parameters are illustrated in Figure 4. As shown in Figure 4, Equation 1 provides a good fit to the experimental data.

2.7 | Analysis of time-dependent viscosities

In order to gain quantified data for comparing the different samples, the time-dependent viscosities were analyzed by fitting to empirical equations. GM exhibits a linear increase in the lin-log plot at short times (Figure 5A), indicative of an exponential increase. Accordingly, this part of the curve can be fitted to $\eta(t) = \eta_{t0}\exp[\Gamma_1 t]$, where t is the time, η_{t0} is the viscosity at zero time, and Γ_1 shows how fast the viscosity is rising. At longer times, a faster upturn of the curve is observed. Empirically this rise could be fitted by a stretched exponential ($\exp[(t/\tau_{GM})^{\beta}]$), where τ_{GM} indicates the time where this rise starts to become significant and the exponent β describes how fast the curve is rising. There is a transition region where both these two effects are influencing the curve. After the transition time, s_1, the initial exponential increase is no longer influencing the viscosity curve. A new single exponential increase (linear in the lin-log figure) is observed at even longer times after the second transition time, s_2. This part of the curve can therefore be fitted to $\eta = \eta_{s2}\frac{\exp[\Gamma_2 t]}{\exp[\Gamma_2 s_2]}$, where η_{s2} is the viscosity at the point where this part of the curve starts at the time s_2. Γ_2 shows how fast the viscosity is rising at this stage, and the term $\exp[\Gamma_2 s_2]$ has to be included since this exponential increase does not start at zero time. Accordingly, the time (t)-dependent viscosities of GM can be described within the three regimes as:

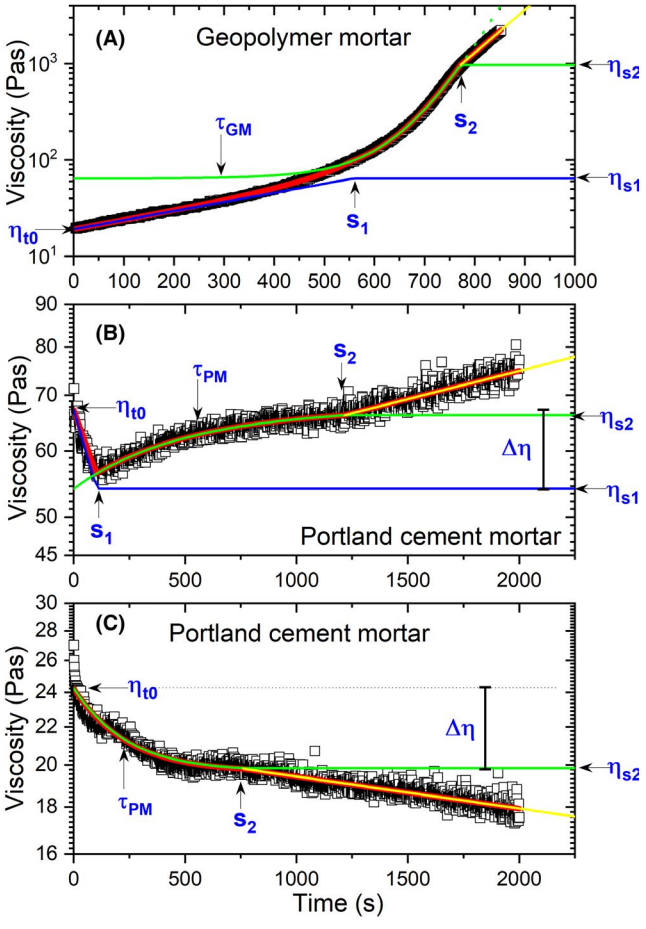

FIGURE 5 Illustration of the fitting parameters. The red lines show the fitted curves (Equation 3 in (A) and Equation 5 in (B and C)). The blue lines are the contributions from the first part of the function, the green lines show the contributions from the second part of the functions, and the yellow lines show the contribution from the third part of the functions. Some of the fitted parameters are indicated in the figure

$$t < s_1 < s_2 \quad \eta(t) = \eta_{t0}\exp[\Gamma_1 t] + \exp\left[\left(\frac{t}{\tau_{GM}}\right)^{\beta}\right] - 1 \qquad (2a)$$

$$s_1 < t < s_2 \quad \eta(t) = \eta_{s1} + \exp\left[\left(\frac{t}{\tau_{GM}}\right)^{\beta}\right] - 1 \qquad (2b)$$

$$s_1 < s_2 < t \quad \eta(t) = \eta_{s2}\frac{\exp[\Gamma_2 t]}{\exp[\Gamma_2 s_2]} \qquad (2c)$$

where $\eta_{s1} = \eta_{t0}\exp[\Gamma_1 s_1]$ and $\eta_{s2} = \eta_{s1} + \exp\left[\left(\frac{s_2}{\tau_{GM}}\right)^{\beta}\right] - 1$. In order to avoid influence of the stretched exponential at short times "-1" is included in Equations 2a and 2b (the stretch exponential goes toward 1 when the time goes toward zero). Combining these equations, the whole viscosity curves were fitted to:

$$\begin{aligned}\eta(t) = {} & \left[\eta_{t0}\exp\left[\Gamma_1\left(s_1 - 0.5\left[s_1 - t + |s_1 - t|\right]\right)\right]\right. \\ & \left. + \exp\left[\left(\frac{s_2 - 0.5\left[s_2 - t + |s_2 - t|\right]}{\tau_{GM}}\right)^{\beta}\right] - 1\right] \\ & \times\left[\frac{\exp\left[\Gamma_2\left(s_2 + 0.5\left[t - s_2 + |s_2 - t|\right]\right)\right]}{\exp[\Gamma_2 s_2]}\right]\end{aligned} \qquad (3)$$

which reduces to Equation 2a, 2b, and 2c within their respective regions. Some of the fitted parameters are illustrated in Figure 5A.

Portland cement mortar exhibits an initial decrease of the viscosity at short times (Figure 5B). As for the initial rise of GM curves, this can be described by $\eta(t) = \eta_{t0}\exp[\Gamma_1 t]$, where

a negative value of Γ_1 indicates that the curve is decreasing. After this, there is a gradual increase toward a plateau value. This part of the curve was found to fit well to $\Delta\eta(1\text{-}\exp(-(t/\tau_{PM})))$, where $\Delta\eta$ is the increase of viscosity during this transition and τ_{PM} is the transition time in the middle of the transition region (see Figure 5B). As for GM, the last part of the curve is linear in the lin-log plot and can be described by $\eta(t)=\eta_{s2}\frac{\exp[\Gamma_2 t]}{\exp[\Gamma_2 s_2]}$. However, for PM, this part of the curve is declining for some of the samples, giving a negative value of Γ_2. Accordingly, the time-dependent viscosities of PM can be described within the three regimes as:

$$t < s_1 < s_2 \quad \eta(t)=\eta_{t0}\exp[\Gamma_1 t]+\Delta\eta-\Delta\eta\exp\left[-\left(\frac{t}{\tau_{PM}}\right)\right] \tag{4a}$$

$$s_1 < t < s_2 \quad \eta(t)=\eta_{s1}+\Delta\eta-\Delta\eta\exp\left[-\left(\frac{t}{\tau_{PM}}\right)\right] \tag{4b}$$

$$s_1 < s_2 < t \quad \eta(t)=\eta_{s2}\frac{\exp[\Gamma_2 t]}{\exp[\Gamma_2 s_2]} \tag{4c}$$

where $\eta_{s1}=\eta_{t0}\exp[\Gamma_1 s_1]$ and $\eta_{s2}=\eta_{s1}+\Delta\eta-\Delta\eta\exp\left[-\left(\frac{s_2}{\tau_{PM}}\right)\right]$. Combining these equations, the whole viscosity curves were fitted to:

$$\eta(t)=\left[\eta_{t0}\exp\left[\Gamma_1\left(s_1-0.5\left[s_1-t+|s_1-t|\right]\right)\right]+\Delta\eta-\Delta\eta\exp\left[-\left(\frac{s_2-0.5\left[(s_2-t)+|s_2-t|\right]}{\tau_{PM}}\right)\right]\right]\times\left[\frac{\exp\left[\Gamma_2\left(s_2+0.5\left[t-s_2+|s_2-t|\right]\right)\right]}{\exp[\Gamma_2 s_2]}\right] \tag{5}$$

which reduces to Equation 4a, 4b and 4c within their respective regions. Some of the fitted parameters are illustrated in Figure 5B.

For some PMs, the viscosities of the second region were found decrease instead of increase (Figure 5C). They can still be fitted with the same equation, giving negative values for $\Delta\eta$ to indicate the decrease. However, these curves had to be fitted without the first decline of Equation 4a, to avoid over-parameterization of the fitting procedure.

3 | RESULTS AND DISCUSSION

3.1 | Shear rate–dependent viscosities

Figure 6 shows the shear rate dependency of mortars. The MPCM is added by replacing the same volume of sand, thereby keeping the solid volume constant. The solid content is also similar for GM and PM. All mortars are shear thinning, with a small plateau at intermediate shear rates. The shear thinning behavior illustrates that there are structures within mortars that can be broken down by shear forces. Some of these structures are easily broken down even with low shear rates, indicating weak forces between the components. When all of these structures are disrupted, the viscosities flatten out in a plateau region. However, when the shear rates become sufficiently high, the shear forces can disrupt stronger agglomerates, and a new shear thinning region is observed. The addition of PE-EVA-PCM to mortars significantly increases the viscosities (Figure 6A,C). This is probably due to the high quantities of water adsorbed onto PE-EVA-PCM compared to the sand it replaces.[18] The viscosities of suspensions increase when the solid content becomes higher.[51,52,53,54]

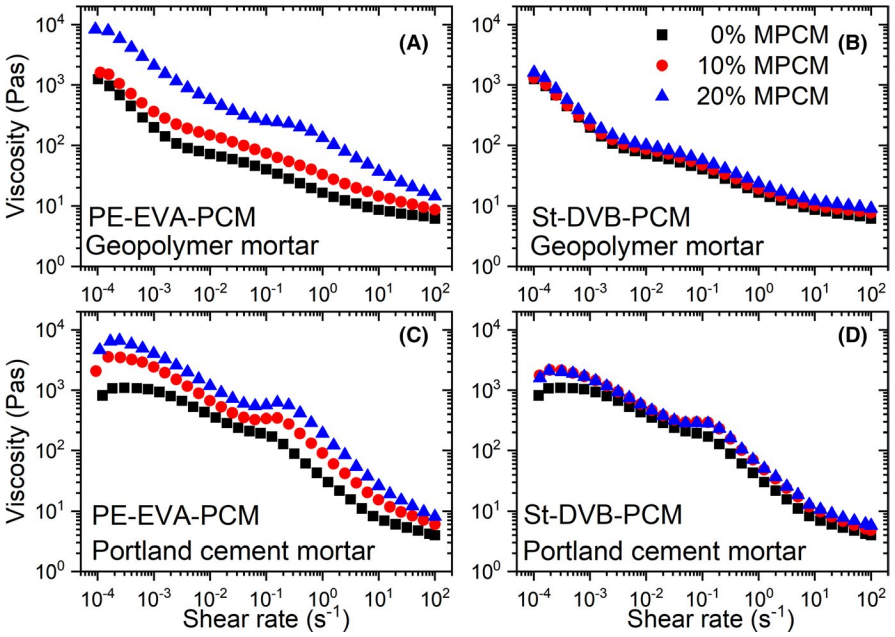

FIGURE 6 Shear rate dependency of the Portland cement mortars and geopolymer mortars containing 0, 10, and 20% of the two MPCMs. Every second data point is shown

Accordingly, effectively removing some of the water by adsorption onto the particles causes the viscosity to rise. St-DVB-PCM is very hydrophobic and adsorbs much less water than PE-EVA-PCM.[18] The viscosities of mortars are therefore only slightly affected by the addition of St-DVB-PCM (Figure 6B,D).

In order to quantify the shear rate dependency of the viscosities, the data were fitted by Equation 1. In the absence of MPCM, GM has a higher zero shear viscosity (η_0) than PM (Figure 7A). This suggests that the workability of the geopolymer is poorer than the Portland cement, which is in agreement with previous findings.[15] The higher initial viscosity of geopolymers compared to Portland cement has been attributed to the larger viscosities of the sodium silicate and sodium hydroxide solutions utilized in the geopolymer recipe.[55] The zero shear viscosity only exhibits a small increase when St-DVB-PCM is added to mortars, while PE-EVA-PCM significantly increases the zero shear viscosity due to its higher water adsorption.[18]

Interestingly, as shown in Figure 7B, the viscosities at the plateau region (η_p) are higher for PM than for GM (the opposite trend of η_0). This illustrates that there are less interactions that are broken down in the low shear rate regime for PMs. η_p increases strongly when the concentration of PE-EVA-PCM is raised. As discussed above, this viscosity increase is probably caused by adsorption of significant amounts of water onto the PE-EVA-PCM microcapsules.[18] The more hydrophobic St-DVB-PCM adsorbs smaller amounts of water, resulting in a more moderate increase of η_p.

At high shear rates, the viscosities approach η_∞ (Figure 7C). No significant differences between the samples are observed in this region. The solid content is nearly the same for all samples, and when the associative interactions are disrupted by high shear forces this causes the viscosities to approach the same values. The minor differences in size distributions are not enough to significantly affect the viscosities at very high shear rates.

The shear rate at which the Newtonian region ends and the first shear thinning regime begin ($\dot{\gamma}_1$) is approximately a decade lower for GM than PM (Figure 7D). In agreement with what was observed for η_p, this shows that the structures in GM are more easily broken down by low shear rates. Interestingly, the addition of MPCM increases $\dot{\gamma}_1$ of GM while the values

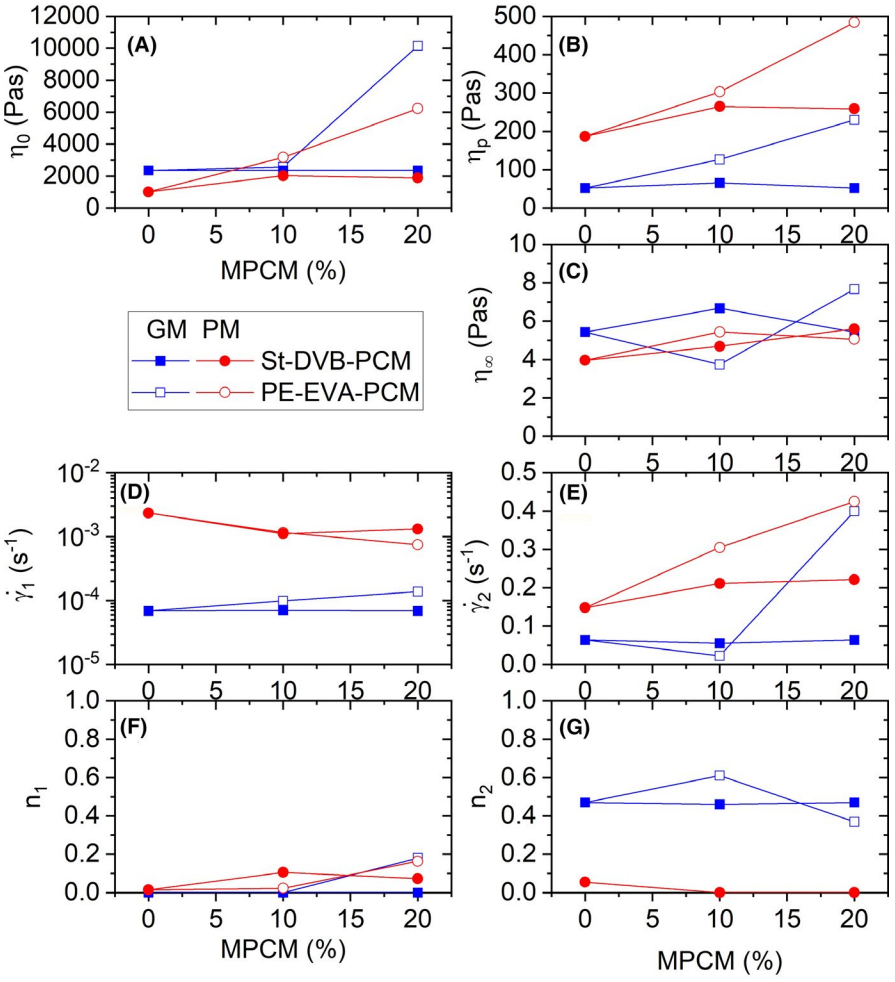

FIGURE 7 The fitted parameters from a double Carreau model (Equation 1) for the geopolymer mortar (GM) and portland cement mortar (PM) as a function of MPCM addition. A, The zero shear viscosity, (B) the viscosity at the plateau region at intermediate shear rates, (C) the viscosity at infinite shear rates, (D) the shear rate where the first shear thinning regions starts, (E) the shear rate where the second shear thinning region starts, (F) the flow behavior index of the first shear thinning region, (G) the flow behavior index of the second shear thinning region. The locations of some of the fitted parameters are illustrated in Figure 4

decline for PM. For GM, this effect is most pronounced for PE-EVA-PCM, suggesting that the reduction of available water within these samples strengthen the interactions between the components. As a result, higher shear forces are needed to break apart the loosely connected structures. The addition of MPCMs decreases $\dot{\gamma}_1$ of PM, suggesting that the amount free water available in the samples is not the main mechanism responsible for the change in $\dot{\gamma}_1$. These findings can be explained by the possibility that portland cement has stronger interactions with sand than with the MPCM.

The shear rate where the second shear thinning regime begins $\dot{\gamma}_2$ is also lowest for GM, although the differences in $\dot{\gamma}_2$ are moderate (Figure 7E). The structures broken apart at these higher shear rates are much stronger that the structures which is disrupted at low shear rates. While shear thinning at low shear rates might indicate loosely flocculated structures, the ability to withstand much stronger shear forces before the viscosity is reduced suggest more compact agglomerates. For both GM and PM, the addition of microcapsules shifts this transition shear rate to higher values. This effect is stronger for PE-EVA-PCM, illustrating that the reduced amount of free water in the samples is a major contributor to this effect.

The flow behavior indexes (n_1 and n_2) show how strongly shear thinning the samples are. A value of 1 indicates no shear thinning, and decreasing values toward zero shows stronger shear thinning (values higher than 1 indicate shear thickening). Figure 7F shows that the first shear thinning regime is strongly shear thinning for all samples. The second shear thinning regime at higher shear rates (Figure 7G) is also strongly shear thinning for PM, while GM exhibit a more moderate shear tinning at this stage. There are no clear effects of MPCM addition on the flow behavior indexes. This indicates that the contribution of the microcapsules in the structures that are broken down by the shear is neglectable in this MPCM concentration range.

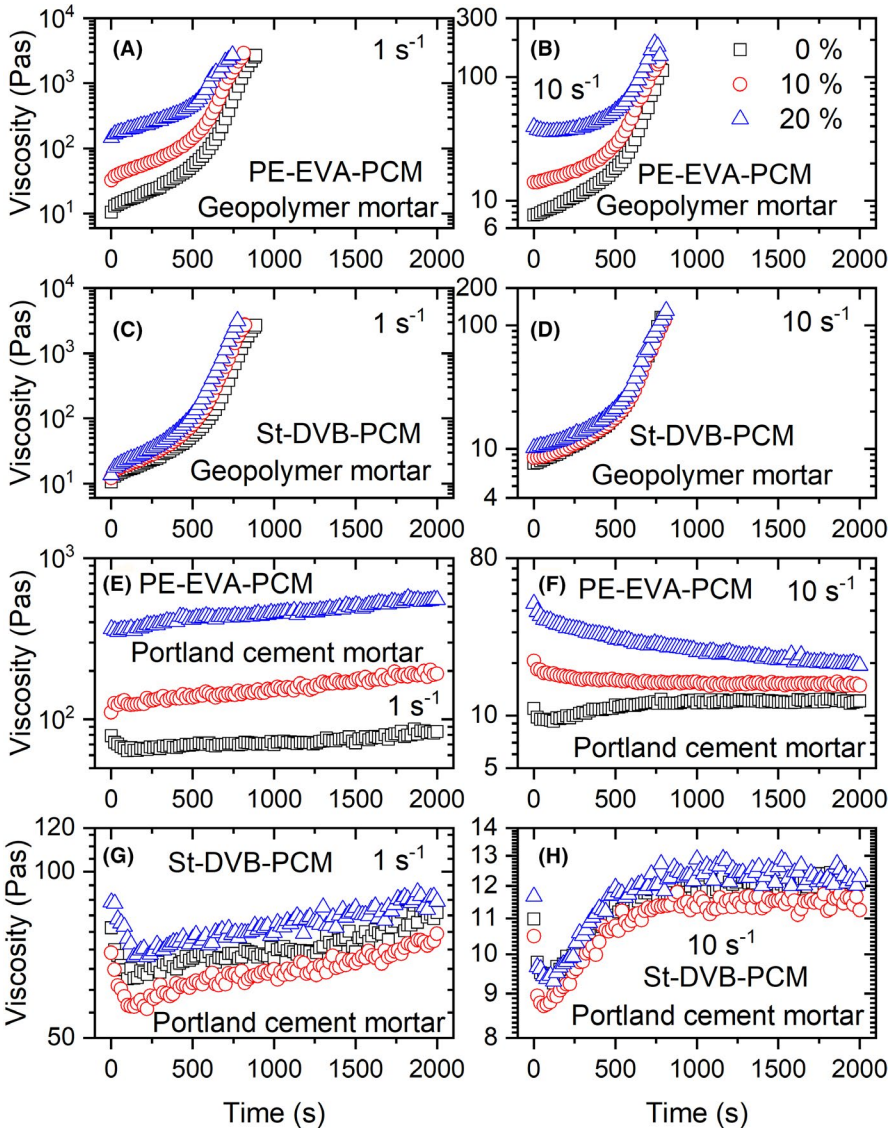

FIGURE 8 Time development of the viscosity of geopolymer mortar containing PE-EVA-PCM at a shear rates of (A) 1 s^{-1} and (B) 10 s^{-1}, geopolymer mortar containing St-DVB-PCM at a shear rates of (C) 1 s^{-1} and (D) 10 s^{-1}, Portland cement mortar containing PE-EVA-PCM at a shear rates of (E) 1 s^{-1} and (F) 10 s^{-1}, Portland cement mortar containing St-DVB-PCM at a shear rates of (G) 1 s^{-1} and (H) 10 s^{-1}. Every 20th data point is shown

3.2 | Time-dependent viscosities

In order to explore the time evolution of the viscosities during the geopolymer and condensation reactions, the samples were measured as a function of time at two different shear rates (1 s^{-1} and 10 s^{-1}). When looking at the time-dependent viscosities, it can be helpful to keep in mind that the geopolymerization process consists of two steps: geopolymer precursors are first formed, after which the 3D geopolymer network is developed from these precursors.[56,57] Portland cement normally undergoes a stage of early cement hydration, followed by a relatively dormant induction period before the main hydration process at later times.[58,59] Accordingly, as can be seen from Figure 8, the time-dependent viscosities of GM and PM behaves very differently. In agreement with Figure 6, PE-EVA-PCM (with a hydrophilic shell) affects the rheological behavior much more than St-DVB-PCM (with a hydrophobic shell).

Unlike GM, PM exhibits a significant amount of noise in the data. In Figure 8, this is most evident for the samples containing St-DVB-PCM. However, a magnification of the data shows that the scattering of the data points also occurs for PE-EVA-PCM. This kind of fluctuating viscosity values are typical for systems where the buildup of larger structures over time is competing with the shear-induced breakup of the same structures.[60] Accordingly, the shear forces of 1 s^{-1} and 10 s^{-1} are breaking down the formation of large structures in Portland cement, thereby slowing down the reaction. The viscosities of the Portland cement are therefore increasing very little during the measurements, and at the highest shear rate the samples containing PE-EVA-PCM actually exhibit a viscosity decrease (which will be discussed in more details in section 3.2.3 below). For GM, the viscosities are strongly increasing over time, without any scattering of the data. This illustrates that the geopolymer reaction products are strong enough that the buildup of larger structures dominates over the shear-induced disruption. To explore the differences between the samples in more detail, we have developed two empirical equations (Equation 3 and Equation 5) to quantify the time-dependent viscosity changes of the samples.

3.2.1 | Initial viscosity

As shown in Figure 9A,B, the viscosity at the start of the reaction (η_{t0}) is lower for GM than for PM, since the initial GM structure is more easily broken down by shear forces than PM (see discussion in connection with Figure 7 above). This is especially evident at the lowest shear rate (1 s^{-1}), since the initial viscosities of GM and PM are approaching each other at high shear rates (Figure 7C). Since St-DVB-PCM adsorbs only slightly more water than the sand it replaces,[18] η_{t0} is nearly constant when the concentration of St-DVB-PCM is raised. PE-EVA-PCM contains some polar groups and therefore adsorbs significantly more water than the sand it replaces.[18] The reduction of free water in the samples causes η_{t0} to become higher when PE-EVA-PCM is added to mortars. Figure 9C,D show the normalized viscosity, η_n (normalized with respect to the corresponding samples without MPCM). Interestingly, the PE-EVA-PCM–induced viscosity increase at the start of the reaction is much more pronounced for GMs than for PMs. This suggests that the viscosity of GMs is more affected by the amount of free water than PMs. It is possible that GM has a higher water demand, and therefore is more sensitive to a further reduction of available water.

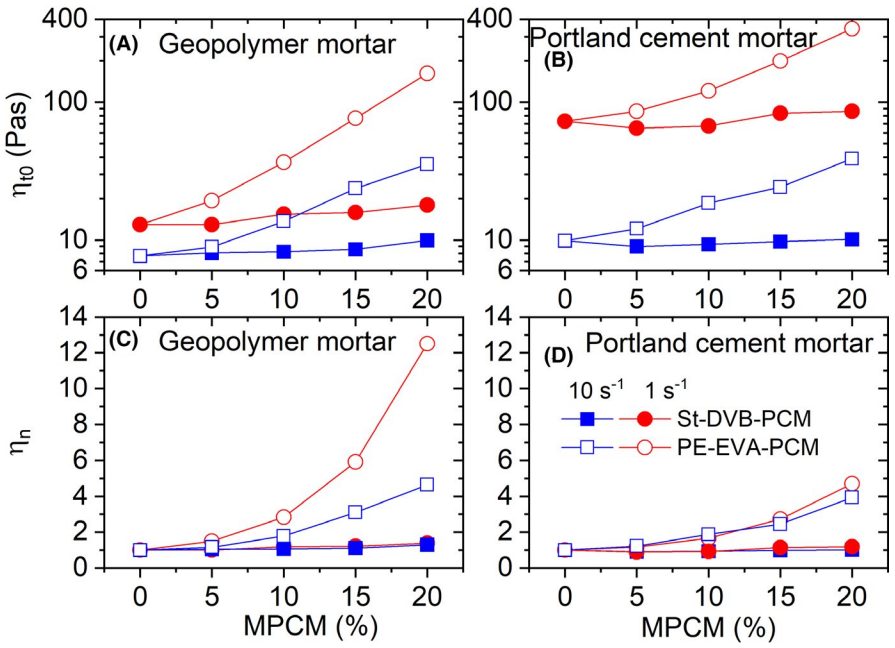

FIGURE 9 Initial viscosity at the start of the measurements (η_{t0}) for (A) geopolymer mortar and (B) Portland cement mortar, and normalized viscosity (η_n) (normalized with respect to the samples without MPCM; $\eta_n = \eta_{t0}/\eta_{t0,\ 0\%\ MPCM}$) of (C) geopolymer mortar and (D) Portland cement mortar containing different amounts of the two MPCMs measured at shear rates of 1 s^{-1} and 10 s^{-1}. The values are the results of fitting the data to Equation 3 (geopolymer mortar) and Equation 5 (Portland cement mortar)

3.2.2 | First viscosity stage

During the first viscosity stage, the time-dependent viscosity follows Equations 2a and 4a for GM and PM, respectively. The rate of viscosity change during the first part of the reaction (Γ_1) is shown in Figure 10A,B. The viscosity of GM (Figure 10A) increases at the start of the reaction ($\Gamma_1 > 0$). This initial slow viscosity increase of geopolymers has been contributed to the formation of geopolymer precursors.[35] This increase is steeper at the lowest shear rate, which is expected since higher shear rates disrupt the reaction process. The addition of PE-EVA-PCM to GM reduces Γ_1. This indicates that the microcapsules slow down the reaction rate, which is in agreement with previous findings.[18] The higher viscosities are probably the main cause of the slower reaction rates.[18] At the highest shear rate, St-DVB-PCM has little effect on Γ_1 for GM. Similar results was also observed for a geopolymer paste (without sand) at the same shear rate.[35] However, at the lowest shear rate (1 s^{-1}), St-DVB-PCM causes Γ_1 of GM to increase, suggesting a faster reaction. Since the addition of St-DVB-PCM only has a minor effect on the initial viscosities (Figure 9A,C), viscosity changes are not a major contributor to Γ_1. However, St-DVB-PCM adsorbs more water than the sand it replaces.[18] The reduction of free water in the sample may increase the concentration of the reactants in the liquid phase, thereby increasing the reaction rate.[35]

The initial increase continues to contribute to the viscosity curve until the time s_1 (see Figure 5A for illustration of s_1). As shown in Figure 10C, s_1 for GMs is not significantly affected by the MPCM concentration. The viscosity at the time s_1 (η_{s1}) is shown in Figure 10E (see Figure 5A for illustration of η_{s1}). The highest shear rate clearly impedes the reaction, as η_{s1} is much higher for the low shear rate (the differences are much less pronounced at the start of the reaction; Figure 9A). η_{s1} becomes higher in the presence of microcapsules. This effect is greatest for PE-EVA-PCM, which exhibits a higher water adsorption that results in raised viscosities (as discussed above). For St-DVB-PCM, the increased reaction rates are contributing to the higher viscosities at this reaction time.

For PM (Figure 10B), the values of Γ_1 are negative, indicating that the viscosity is decreasing during the initial stage. The viscosity reduction is probably due to the shear forces disrupting agglomerates formed within the samples. At a shear rate of 10 s^{-1}, the viscosity of the samples containing PE-EVA-PCM continues to decline after the initial stage (Figure 8F). These curves were therefore fitted without the first part of Equation 4a (and therefore without Γ_1), to avoid overparameterization of the fitting procedure. At the low shear rate (1 s^{-1}), the same samples did not exhibit any initial

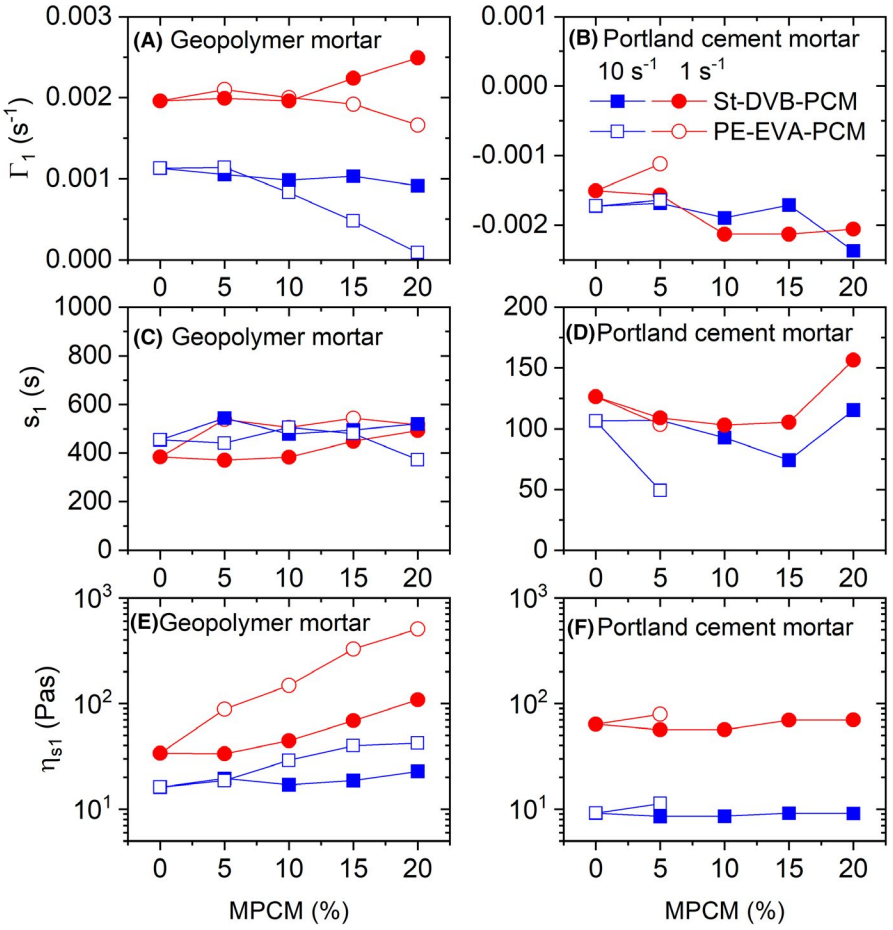

FIGURE 10 (A) The rate of viscosity change at the initial stage (Γ_1) for geopolymer mortar, (B) the rate of viscosity change at the initial stage (Γ_1) for Portland cement mortar, (C) the time s_1 where the initial increase is no longer contributing to the geopolymer mortar viscosity curves, (D) the time s_1 where the initial decline of the viscosity of Portland cement mortar stops, (E) the viscosity at s_1 for geopolymer mortar, (F) the viscosity at s_1 for Portland cement mortar. The values are the results of fitting the data to Equation 3 (geopolymer mortar) and Equation 5 (Portland cement mortar)

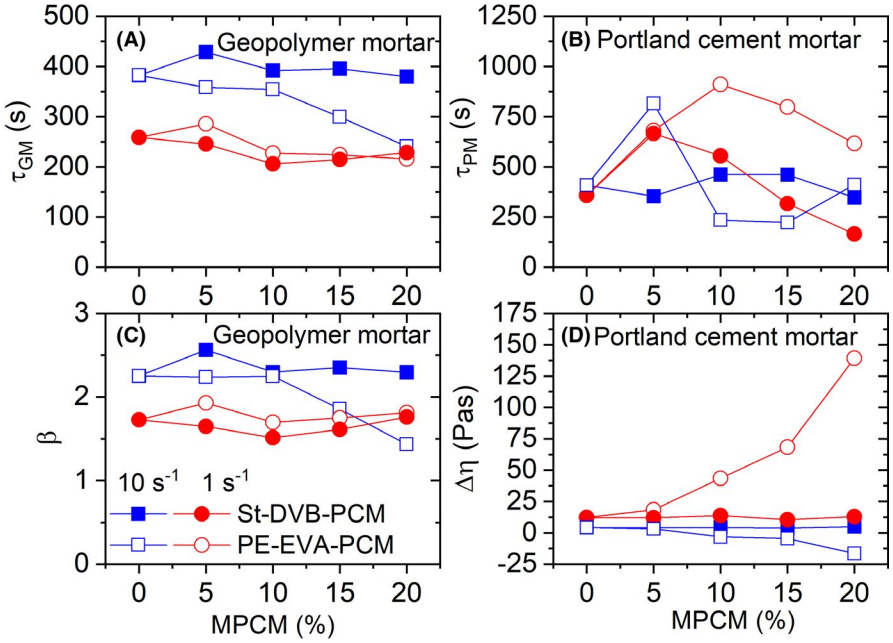

FIGURE 11 (A) The transition time (τ_{GM}) for geopolymer mortar, (B) the transition time (τ_{GM}) for Portland cement mortar, (C) the exponent β for geopolymer mortar, (D) the viscosity change $\Delta\eta$ for Portland cement mortar. The values are the results of fitting the data to Equation 3 (geopolymer mortar) and Equation 5 (Portland cement mortar)

decline (Figure 8E), and were therefore also fitted without the first part of Equation 4a. The absence of an initial viscosity reduction at low shear rates illustrate that the shear forces are not strong enough to break apart the agglomerated structures.

The initial decrease stops at the time s_1 (see Figure 5B for illustration of s_1). As shown in Figure 10D, for PM s_1 is occurring after just a few minutes. Accordingly, this viscosity reduction is probably caused by the breakdown of agglomerates already present in the samples before the reaction starts. The viscosities at the time s_1 (η_{s1}) are the minimum viscosities of the curves (see Figure 5B for illustration of η_{s1}). η_{s1} is much lower for the highest shear rate, since more agglomerates can be broken apart by the stronger shear forces.

3.2.3 | Intermediate viscosity stage

During the intermediate viscosity stage, the time-dependent viscosity follows Equations 2b and 4b for GM and PM, respectively. The transition time τ_{GM} (Figure 11A) shows where the steeper viscosity increase starts for GMs (see Figure 5A for illustration of τ_{GM}). This steeper rise in viscosity is caused by the formation of a 3D geopolymer network.[35] The transition time is delayed when the shear rate is increased (Figure 11A), since the higher shear forces impede the reaction. At the lowest shear rate (1 s^{-1}), there is very little change in τ_{GM} when the microcapsule concentration is raised. The addition of St-DVB-PCM at the higher shear rate of 10 s^{-1} does not significantly affect τ_{GM}. However, at the highest shear rate, τ_{GM} decreases for the samples containing PE-EVA-PCM. Accordingly, the start of the formation of the 3D geopolymer network starts earlier although the formation of the geopolymer precursors is slowed down (Figure 10A). The main difference between adding the two types of microcapsules is that PE-EVA-PCM adsorbs much more water than St-DVB-PCM.[18] The water adsorption causes a higher effective concentration of the reactants in the liquid phase. It is possible that the combination of a higher collision rate of the reactants when the shear rate is raised and the increased effective concentration of the geopolymer precursors causes the observed decline of τ_{GM} for PE-EVA-PCM at 10 s^{-1}.

The exponent β for GMs (Figure 11C) is a measure of how steep the upturn of the viscosity curve is during the intermediate stage. A higher value of β indicates a steeper rise of the curves. Interestingly, at this intermediate stage the viscosity of GMs has a steeper increase at the highest shear rate. Since the higher shear rate shift the start of this regime to longer times (Figure 11A), more geopolymer precursors might have time to form although they are forming slower (Figure 10A). If more precursors are present, the formation of the 3D geopolymer network would be faster causing a higher value of β. As for τ_{GM}, the addition of St-DVB-PCM or PE-EVA-PCM at a low shear rate does not significantly affect β. However, at the high shear rate (10 s^{-1}), β clearly decreases when the concentration of PE-EVA-PCM is raised. This is in agreement with the declining values of both Γ_1 and τ_{GM} of this sample. Since the geopolymer precursors are formed more slowly (Figure 10A) and the start of the formation of the 3D geopolymer network occurs earlier (Figure 11C), less geopolymer precursors are present and the formation of the 3D geopolymer network is therefore slower.

The transition time τ_{PM} (Figure 11B) is the transition time in the middle of the intermediate viscosity change of PM (see Figure 5B,C for illustration of τ_{PM}). This transition time goes through a broad maximum when the microcapsule concentration is raised. An increased water content results in a higher degree of cement hydration at long times.[61,62] However, during

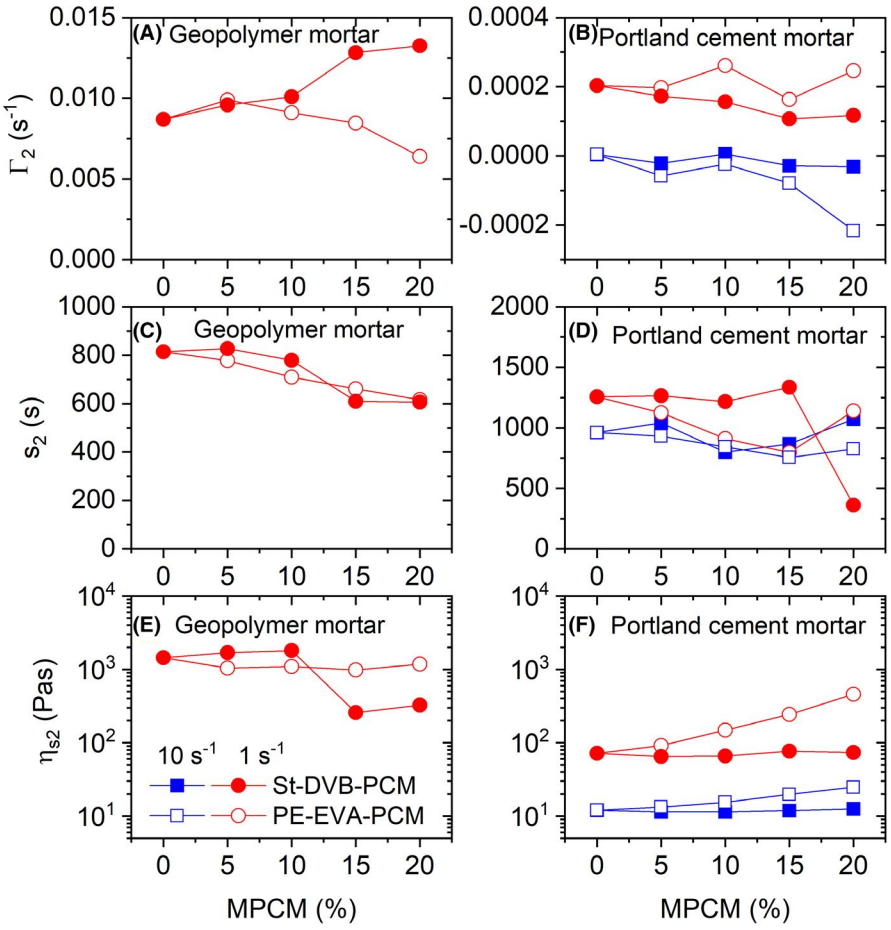

FIGURE 12 (A) The rate of viscosity increase in the final stage (Γ_2) for geopolymer mortar, (B) the rate of viscosity increase in the final stage (Γ_2) for portland cement mortar. (C) the time s_2 where the final viscosity stage starts for the geopolymer mortar, (D) the time s_2 where the final viscosity stage starts for the portland cement mortar, (E) the viscosity at s_2 for geopolymer mortar, (F) the viscosity at s_2 for portland cement mortar. The values are the results of fitting the data to Equation 3 (geopolymer mortar) and Equation 5 (Portland cement mortar)

the early stages of the hydration process, a reduction in the w/c ratio speeds up the cement hydration.[62,63,64] This has been contributed to larger initial particle spacing for high w/c ratios,[63] and a promotion of the dissolution of the anhydrous phase due to a larger concentration of alkali ions in the water at low w/c ratios.[62] Accordingly, the addition of water-adsorbing microcapsules can speed up the reaction rate at this stage of the Portland cement reaction. In contrast, the increased viscosities at high MPCM concentrations (Figure 8) might slow down the reaction rates.[65,66,67] The observed variations in τ_{PM} are probably a result of these competing mechanisms, combined with the disrupting influence of the applied shear forces.

Figure 11D shows the viscosity change ($\Delta\eta$) of PM during this intermediate stage (see Figure 5B,C for illustration of $\Delta\eta$). The addition of St-DVB-PCM does not significantly affect these values. For the samples containing St-DVB-PCM, $\Delta\eta$ is slightly higher at the lowest shear rate, since higher shear rates disrupts the hydration reaction. At the lowest shear rate, $\Delta\eta$ is strongly increasing when PE-EVA-PCM is added to PM. This is probably due to the faster hydration rate discussed above. At the highest shear rate, raising the PE-EVA-PCM concentration causes $\Delta\eta$ to decline and assume negative values, that is, the viscosity is decreasing (Figure 8F). The high shear rates are breaking apart agglomerates within the samples. Since PE-EVA-PCM adsorbs high amounts of water, the initial viscosities are increased (Figure 8F). This indicates that there are more agglomerates available for disruption when the PE-EVA-PCM concentration is raised. Accordingly, there are more structures present that can be broken down by the high shear forces, causing the observed decline of $\Delta\eta$ toward more negative values.

3.2.4 | Final viscosity stage

During the final viscosity stage, the time-dependent viscosity follows Eqa. 2c and 4c for GM and PM, respectively. Figure 12A shows how fast the viscosity of GM is increasing during the final stage. At this stage, the curves are actually less steep than during the intermediate stage (Figure 5A). A visual inspection of the samples revealed that the transition is due to the creation of a split of the sample within the measuring cell into an inner cylinder (surrounding the rotating stirrer) and an outer shell (stuck to the walls of the measuring cylinder). This effect is only evident for the lowest shear rate (1 s^{-1}), while the higher shear rate (10 s^{-1}) does not exhibit this transition. The faster formation of a 3D geopolymer network at 10 s^{-1} (discussed above) probably prevents the samples from splitting into two different sections. Accordingly, Γ_2 is mainly reflecting artefacts due to the split sample.

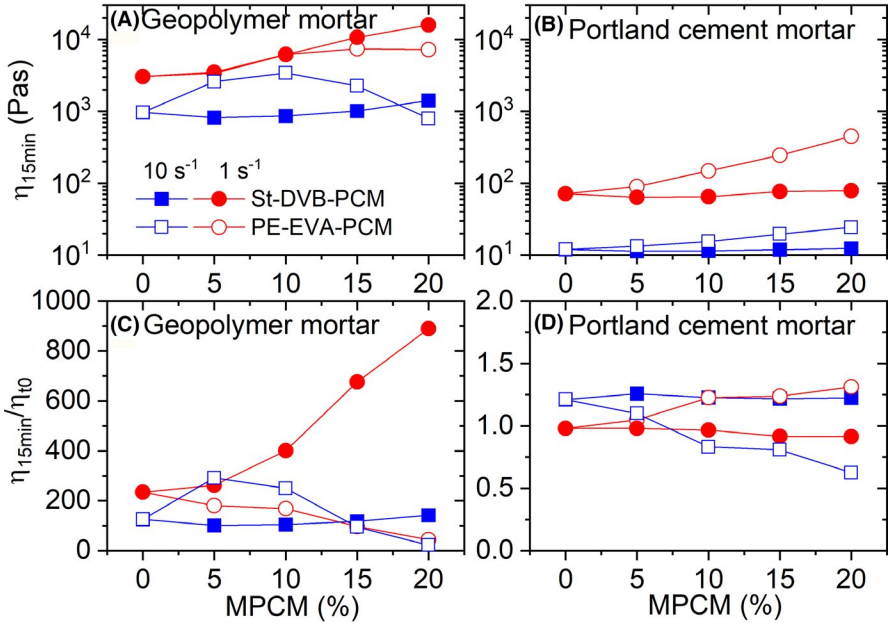

FIGURE 13 Viscosity after 15 min at shear rates of 1 s^{-1} and 10 s^{-1} (η_{15min}) for (A) geopolymer mortar and (B) Portland cement mortar, and the same values normalized by the corresponding values at the start of the reaction (η_{15min}/η_{t0}) for (C) geopolymer mortar and (D) Portland cement mortar containing different amounts of the two MPCMs. The values are the results of fitting the data to Equation 3 (geopolymer mortar) and Equation 5 (Portland cement mortar)

The time s_2 (see Figure 5A for illustration of s_2) illustrates the time when GM splits into an inner and an outer cylinder (Figure 12C). There is no significant difference between St-DVB-PCM and PE-EVA-PCM, but the split seems to occur at earlier times when more microcapsules are added to GM. The viscosities of GM when the sample splits, η_{s2}, (see Figure 5A for illustration of η_{s2}) is independent of MPCM concentration for PE-EVA-PCM (Figure 12E). At low concentrations of St-DVB-PCM, η_{s2} is close to that of PE-EVA-PCM, while it is significantly lower at higher concentrations. Accordingly, it seems like the samples break when they reach a sufficiently high stress (since the samples are measured at a constant shear rate, a constant viscosity equals a constant stress (σ); $\sigma = \dot{\gamma}\eta$). This might occur because the stirrer is no longer able to move the sample that is outside the diameter of the stirrer. The addition of high amounts of the hydrophobic St-DVB-PCM shifts this fracturing viscosity and stress to lower values. This is possibly due to poor interaction between these hydrophobic microcapsules and GM matrix.

Figure 12D shows the time, s_2, where the transition to the last stage occur for PM (see Figure 5B,C for illustration of s_2). Unlike GM, PM does not split, and the last stage reflects a real effect of the samples. The transition time s_2 is probably related to the onset of the induction period between the early cement hydration and the main hydration reaction at later times.[58,59] The onset of the induction period is thought to be related to a slow down of the dissolution process due to low undersaturation.[58,59] At the highest shear rate (10 s^{-1}), there is little effect on the transition time s_2 with MPCM addition. In the absence of microcapsules, the transition time is shifted to longer times when the shear rate is decreased. A higher shear rate will contribute to disruption of agglomerates into smaller entities, leading to a larger exposed surface area. The dissolution process might therefore become faster at high shear rates, causing low undersaturation at shorter times. The addition of PE-EVA-PCM at a shear rate of 1 s^{-1} causes s_2 to decrease. This might be related to adsorption of water onto the microcapsules, thereby causing a low undersaturation at an earlier stage. Except for the highest concentration, St-DVB-PCM (which adsorbs much less water than PE-EVA-PCM) has little effect on s_2.

Γ_2 for PM (Figure 12B) is a parameter that reflects how fast the viscosity is growing (positive values) or decreasing (negative values) during the last stage of the viscosity measurements. During the induction period, the cement hydration is progressing very slowly, which is the reason for the very slow viscosity increase even under a low shear rate. At the highest shear rate (10 s^{-1}), the viscosity is decreasing, indicating that the shear rate is high enough to break apart structures within the samples faster than the hydration reaction can build up new structures.

Figure 12F shows the viscosity, η_{s2}, at the transition point (see Figure 5B,C for illustration of η_{s2}). η_{s2} is independent of the addition of St-DVB-PCM, but increasing with PE-EVA-PCM concentration. This is probably due to the adsorption of water onto the PE-EVA-PCM particles. In addition, η_{s2} is lower for the higher shear rate, since higher shear rates will break apart agglomerates within the samples.

3.2.5 | Viscosities after 15 minutes

After 15 minutes, the viscosities of GMs have increased considerably, while PMs are still relatively close to the original values (Figure 13). This might indicate that the employed

shear rates are having a stronger disrupting effect on the Portland cement reactions than on the geopolymer reaction rate. However, it could also reflect that the viscosity development of PMs is slower than GMs. It is known that the setting time of Portland cement paste is much slower than geopolymer paste,[68] and accordingly it is reasonable to assume that the viscosity development could also be much slower. Figure 13C,D depicts the viscosities after 15 minutes normalized with respect to the corresponding values at the start of the reaction (η_{15min}/η_{t0}), illustrating how much the viscosities change during the first 15 minutes of reaction. In the absence of microcapsules, the viscosity of GMs increases more at the lowest shear rate, since higher shear forces will impede the reaction.

While St-DVB-PCM do not seem to affect the viscosity increase of GM after 15 minutes when measured at a shear rate of 10 s^{-1}, the same samples increase sharply with St-DVB-PCM concentration when the measurements are conducted at a lower shear rate of 1 s^{-1} (Figure 13C). This suggests that St-DVB-PCM speeds up the geopolymer reaction rate, but this effect is suppressed when the samples are subjected to sufficiently high shear forces. The geopolymer reaction is a two-step process. First, the aluminosilicates react with the alkaline activator, forming geopolymer precursors. Second, these monomers also react with the alkaline activator forming the 3D geopolymer structure.[56,57] The first step only causes a moderate viscosity increase, while the second step causes a significantly steeper growth of the viscosities.[35] Interestingly, it seems that the much higher viscosities for the samples containing high amounts of St-DVB-PCM at 1 s^{-1} is mainly due to a faster reaction rate during the first step of the process (increasing Γ_1 in Figure 10A), since the onset of the second stage (τ_{GM} in Figure 11A) and how steeply the viscosity is raising during the second stage (β in Figure 11C) is changing very little with the addition of St-DVB-PCM.

Unlike St-DVB-PCM, increasing the amount of PE-EVA-PCM seem to slow down the reaction rate at a shear rate of 1 s^{-1} and go through a maximum at 10 s^{-1}. As discussed above, PE-EVA-PCM slows down the reaction rate during the initial stage of the geopolymer reaction (Γ_1 in Figure 10A). At a shear rate of 1 s^{-1} this is the main contributing effect to the decreasing values in Figure 13C, since τ_{GM} (Figure 11A) and β (Figure 11C) are nearly constant. At a shear rate of 10 s^{-1}, the reaction rate is also reduced during the second stage (decreasing β in Figure 11C). However, the onset of the second stage occurs earlier (τ_{GM} in Figure 11A is declining), which will contribute to a faster viscosity increase. The overall effect is therefore the observed maximum in the η_{15min}/η_{t0} values.

For PM (Figure 13D), the viscosities change very little during the first 15 minutes of the reaction, probably due to the slower reaction rate of Portland cement combined with a more pronounced shear-induced breakup of the newly formed structures within the samples. Interestingly, in the absence of microcapsules, the viscosity increases more during the first 15 minutes at 10 s^{-1} than at the lower shear rate of 1 s^{-1}. This is probably related to the initial much higher viscosities at 1 s^{-1} (Figure 9B). Accordingly, there are initially more unbroken agglomerates present at 1 s^{-1}, and the initial decline at short times therefore lasts longer (s_1 in Figure 10D). The addition of the hydrophobic St-DVB-PCM does not change η_{15min}/η_{t0} for PM, suggesting that these microcapsules do not influence the reaction rate. However, PE-EVA-PCM causes a reduction of η_{15min}/η_{t0} at high shear rates, and an increase at low shear rates (Figure 13D). This is in agreement with the faster reaction rates at low shear rates and the shear-induced disruption of the samples at high shear rates discussed in connection with Figure 11 above.

4 | CONCLUSIONS

- The shear rate dependency of the viscosity of both GM and PM, where 0-20 vol% of the sand was replaced with thermoregulating microcapsules, was found to fit well to a double Carreau model.
- Empirical equations were developed to express the time-dependent viscosities of both GM and PM. The fitted parameters from these equations can be used to quantify how fast the geopolymerization and hydration reactions are proceeding at different shear rates and at various microcapsule concentrations.
- Although the zero shear viscosities of GMs are higher than for PMs, the initial structures within GMs are more easily broken apart by shear forces than PMs. However, the geopolymer reaction proceeds much faster than the Portland cement hydration, and the geopolymer reaction products are less affected by shear forces than the Portland cement hydration products.
- Both the geopolymer reaction and the Portland cement hydration are impeded by high shear forces. The viscosities are much more affected by the addition of the relatively hydrophilic PE-EVA-PCM than the hydrophobic St-DVB-PCB, due to the higher water adsorption onto PE-EVA-PCM.
- The viscosity of GM increases relatively slowly during the initial stage when the geopolymer precursors are formed, and much faster during the next stage when a 3D-geopolymer network is developed.
- The viscosities of PMs decrease during the first few minutes, due to disruption of agglomerated structures already present in the samples. After this, the initial hydration process increases the viscosities. However, there is a competition between the buildup of hydration products and the shear-induced disruption of the structures within the samples. Accordingly, at the highest shear rate

the overall effect for some of the samples is a viscosity decline.

- When PMs reach the intermediate induction period, the hydration reaction proceeds much slower. Accordingly, the viscosity rise is very modest, and several samples exhibit a shear-induced viscosity reduction.
- The influence of the microcapsules on the viscosity development and reaction rates of GM and PM are quite complex since they might both speed up and slow down the different stages of the geopolymer and hydration reactions.

ACKNOWLEDGMENTS

We gratefully acknowledge funding from the Research Council of Norway, project number 238198. The authors acknowledge Fundación Séneca Agencia de Ciencia y Tecnología de la Región de Murcia "Ayuda a las Unidades y Grupos de Excelencia Científica de la Región de Murcia (Programa Séneca 2014)" (Grant # 19877/GERM/14) for financial support.

ORCID

Shima Pilehvar https://orcid.org/0000-0003-1589-2825
Manuel Carmona https://orcid.org/0000-0002-1464-5067
Ramón Pamies https://orcid.org/0000-0002-3950-8915
Anna-Lena Kjøniksen https://orcid.org/0000-0003-4864-4043

REFERENCES

1. Davidovits J. Geopolymer chemistry and applications. Saint-Quentin, France: Institute Géopolymère. 2011. p. 612.
2. Duxson P, Provis JL, Lukey GC, van Deventer JSJ. The role of inorganic polymer technology in the development of 'green concrete'. Cem Concr Res. 2007;37(12):1590–7.
3. Ling T-C, Poon C-S. Use of phase change materials for thermal energy storage in concrete: an overview. Constr Build Mater. 2013;46:55–62.
4. Whiffen TR, Riffat SB. A review of PCM technology for thermal energy storage in the built environment: Part I. Int J Low-Carbon Technol. 2013;8(3):147–58.
5. McLaggan MS, Hadden RM, Gillie M. Flammability assessment of phase change material wall lining and insulation materials with different weight fractions. Energy Build. 2017;153(Supplement C):439–47.
6. Szczotok AM, Carmona M, Kjøniksen A-L, Rodriguez JF. Equilibrium adsorption of polyvinylpyrrolidone and its role on thermoregulating microcapsules synthesis process. Colloid Polym Sci. 2017;295(5):783–92.
7. Zhang GH, Zhao CY. Thermal and rheological properties of microencapsulated phase change materials. Renew Energ. 2011;36(11):2959–66.
8. Bentz DP, Turpin R. Potential applications of phase change materials in concrete technology. Cem Concr Compos. 2007;29(7):527–32.
9. Cao VD, Pilehvar S, Salas-Bringas C, Szczotok AM, Bui TQ, Carmona M, et al. Thermal performance and numerical simulation of geopolymer concrete containing different types of thermoregulating materials for passive building applications. Energy Build. 2018;173:678–88.
10. Cao VD, Pilehvar S, Salas-Bringas C, Szczotok AM, Bui TQ, Carmona M, et al. Thermal analysis of geopolymer concrete walls containing microencapsulated phase change materials for building applications. Sol Energy. 2019;178:295–307.
11. Cao VD, Bui TQ, Kjøniksen A-L. Thermal analysis of multi-layer walls containing geopolymer concrete and phase change materials for building applications. Energy. 2019;186:115792.
12. Cao VD, Pilehvar S, Salas-Bringas C, Szczotok AM, Rodriguez JF, Carmona M, et al. Microencapsulated phase change materials for enhancing the thermal performance of Portland cement concrete and geopolymer concrete for passive building applications. Energy Convers Manage. 2017;133:56–66.
13. Cao VD, Pilehvar S, Salas-Bringas C, Szczotok AM, Valentini L, Carmona M, et al. Influence of microcapsule size and shell polarity on thermal and mechanical properties of thermoregulating geopolymer concrete for passive building applications. Energy Convers Manage. 2018;164:198–209.
14. Hunger M, Entrop AG, Mandilaras I, Brouwers HJH, Founti M. The behavior of self-compacting concrete containing micro-encapsulated phase change materials. Cem Concr Compos. 2009;31(10):731–43.
15. Pilehvar S, Cao VD, Szczotok AM, Valentini L, Salvioni D, Magistri M, et al. Mechanical properties and microscale changes of geopolymer concrete and Portland cement concrete containing micro-encapsulated phase change materials. Cem Concr Res. 2017;100:341–9.
16. Talha Junaid M, Kayali O, Khennane A, Black J. A mix design procedure for low calcium alkali activated fly ash-based concretes. Constr Build Mater. 2015;79:301–10.
17. Sanfelix SG, Zea-García JD, Londono-Zuluaga D, Santacruz I, De la Torre AG, Kjøniksen A-L. Hydration development and thermal performance of calcium sulphoaluminate cements containing microencapsulated phase change materials. Cem Concr Res. 2020;132:106039.
18. Pilehvar S, Cao VD, Szczotok AM, Carmona M, Valentini L, Lanzón M, et al. Physical and mechanical properties of fly ash and slag geopolymer concrete containing different types of micro-encapsulated phase change materials. Constr Build Mater. 2018;173:28–39.
19. Pacheco-Torgal F, Castro-Gomes J, Jalali S. Alkali-activated binders: a review. Part 2. About materials and binders manufacture. Constr Build Mater. 2008;22(7):1315–22.
20. Kong D, Su Y, Du X, Yang Y, Wei S, Shah SP. Influence of nano-silica agglomeration on fresh properties of cement pastes. Constr Build Mater. 2013;43:557–62.
21. Kawashima S, Hou P, Corr DJ, Shah SP. Modification of cement-based materials with nanoparticles. Cem Concr Compos. 2013;36:8–15.
22. Senff L, Labrincha JA, Ferreira VM, Hotza D, Repette WL. Effect of nano-silica on rheology and fresh properties of cement pastes and mortars. Constr Build Mater. 2009;23(7):2487–91.
23. Qian Y, Ma S, Kawashima S, De Schutter G. Rheological characterization of the viscoelastic solid-like properties of fresh cement pastes with nanoclay addition. Theor Appl Fract Mech. 2019;103:102262.
24. Costa EBC, Cardoso FA, John VM. Influence of high contents of limestone fines on rheological behaviour and bond strength of cement-based mortars. Constr Build Mater. 2017;156:1114–26.
25. Wang Q, Wang J, Lu C-X, Cui X-Y, Li S-Y, Wang X. Rheological behavior of fresh cement pastes with a graphene oxide additive. New Carbon Mater. 2016;31(6):574–84.

26. Zhong J, Zhou G-X, He P-G, Yang Z-H, Jia D-C. 3D printing strong and conductive geo-polymer nanocomposite structures modified by graphene oxide. Carbon. 2017;117:421–6.
27. Skripkiunas G, Karpova E, Barauskas I, Bendoraitiene J, Yakovlev G. Rheological properties of cement pastes with multiwalled carbon nanotubes. Adv Mater Sci Eng. 2018;2018:1–13.
28. Sun K, Wang S, Zeng L, Peng X. Effect of styrene-butadiene rubber latex on the rheological behavior and pore structure of cement paste. Compos B. 2019;163:282–9.
29. Lv J, Du Q, Zhou T, He Z, Li K. Fresh and mechanical properties of self-compacting rubber lightweight aggregate concrete and corresponding mortar. Adv Mater Sci Eng. 2019;2019:1–14.
30. Jiao D, Shi C, Yuan Q, Zhu D, De Schutter G. Effects of rotational shearing on rheological behavior of fresh mortar with short glass fiber. Constr Build Mater. 2019;203:314–21.
31. Yunsheng Z, Wei S, Zongjin L, Xiangming Z, Eddie , Chungkong C Impact properties of geopolymer based extrudates incorporated with fly ash and PVA short fiber. Constr Build Mater. 2008;22(3):370–83.
32. Choi S-J, Choi J-I, Song J-K, Lee BY. Rheological and mechanical properties of fiber-reinforced alkali-activated composite. Constr Build Mater. 2015;96:112–8.
33. Westerholm M, Lagerblad B, Silfwerbrand J, Forssberg E. Influence of fine aggregate characteristics on the rheological properties of mortars. Cem Concr Compos. 2008;30(4):274–82.
34. Coppola L, Coffetti D, Lorenzi S. Cement-based renders manufactured with phase-change materials: applications and feasibility. Adv Mater Sci Eng. 2016;2016:1–6.
35. Cao VD, Pilehvar S, Salas-Bringas C, Szczotok AM, Do NBD, Le HT, et al. Influence of microcapsule size and shell polarity on the time-dependent viscosity of geopolymer paste. Ind Eng Chem Res. 2018;57(29):9457–64.
36. Sanfelix SG, Santacruz I, Szczotok AM, Belloc LMO, De la Torre AG, Kjøniksen A-L. Effect of microencapsulated phase change materials on the flow behavior of cement composites. Constr Build Mater. 2019;202:353–62.
37. Ferraris CF. Measurement of the rheological properties of high performance concrete: State of the art report. J Res Natl Inst Stand Technol. 1999;104(5):461–78.
38. Roussel N. Steady and transient flow behaviour of fresh cement pastes. Cem Concr Res. 2005;1656–64.
39. Quanji Z, Lomboy GR, Wang K. Influence of nano-sized highly purified magnesium alumino silicate clay on thixotropic behavior of fresh cement pastes. Constr Build Mater. 2014;69:295–300.
40. Borreguero AM, Valverde JL, Rodriguez JF, Barber AH, Cubillo JJ, Carmona M. Synthesis and characterization of microcapsules containing Rubitherm (R) RT27 obtained by spray drying. Chem Eng J. 2011;166(1):384–90.
41. Chhabra RP. Non-Newtonian fluids: An introduction. New York: Springer; 2010. p. 1.
42. Garakani AHK, Mostoufi N, Sadeghi F, Hosseinzadeh M, Fatourechi H, Sarrafzadeh MH, et al. Comparison between different models for rheological characterization of activated sludge, Iran. J Environ Health Sci Eng. 2011;8(3):255–64.
43. Lee JK, Ko J, Kim YS. Rheology of fly ash mixed tailings slurries and applicability of prediction models. Minerals. 2017;7(9):165.
44. Tao C, Kutchko BG, Rosenbaum E, Massoudi M. A review of rheological modeling of cement slurry in oil well applications. Energies. 2020;13(3):570.
45. Papo A. Rheological models for gypsum plaster pastes. Rheol Acta. 1988;27(3):320–5.
46. Choi BI, Kim JH, Shin TY. Rheological model selection and a general model for evaluating the viscosity and microstructure of a highly-concentrated cement suspension. Cem Concr Res. 2019;123:105775.
47. Benyounes K. Rheological behavior of cement-based grout with Algerian bentonite. SN Appl Sci. 2019;1(9):1037.
48. Bouvet A, Ghorbel E, Bennacer R. The mini-conical slump flow test: analysis and numerical study. Cem Concr Res. 2010;40(10):1517–23.
49. Cardone F, Ferrotti G, Frigio F, Canestrari F. Influence of polymer modification on asphalt binder dynamic and steady flow viscosities. Constr Build Mater. 2014;71:435–43.
50. Carreau PJ, MacDonald IF, Bird RB. A nonlinear viscoelastic model for polymer solutions and melts—II. Chem Eng Sci. 1968;23(8):901–11.
51. Nzihou A, Attias L, Sharrock P, Ricard A. A rheological, thermal and mechanical study of bone cement—from a suspension to a solid biomaterial. Powder Technol. 1998;99(1):60–9.
52. Feys D, Verhoeven R, De Schutter G. Why is fresh self-compacting concrete shear thickening? Cem Concr Res. 2009;39(6):510–23.
53. Ma K, Feng J, Long G, Xie Y. Effects of mineral admixtures on shear thickening of cement paste. Constr Build Mater. 2016;126:609–16.
54. Li H, Huang F, Xie Y, Yi Z, Wang Z. Effect of water-powder ratio on shear thickening response of SCC. Constr Build Mater. 2017;131:585–91.
55. Deb PS, Nath P, Sarker PK. The effects of ground granulated blast-furnace slag blending with fly ash and activator content on the workability and strength properties of geopolymer concrete cured at ambient temperature. Mater Des. 2014;62:32–9.
56. Wang K-T, Tang Q, Cui X-M, He Y, Liu L-P. Development of near-zero water consumption cement materials via the geopolymerization of tektites and its implication for lunar construction. Sci Rep. 2016;6:29659.
57. Mustafa Al Bakri AM, Kamarudin H, Bnhussain M, Khairul Nizar I, Mastura WIW. Mechanism and chemical reaction of fly ash geopolymer cement- a review. J Asian Sci Res. 2011;1:247–53.
58. Juilland P, Gallucci E, Flatt R, Scrivener K. Dissolution theory applied to the induction period in alite hydration. Cem Concr Res. 2010;40(6):831–44.
59. Scrivener KL, Juilland P, Monteiro PJM. Advances in understanding hydration of Portland cement. Cem Concr Res. 2015;78:38–56.
60. Maleki A, Kjøniksen A, Nyström B. Effect of shear on intramolecular and intermolecular association during cross-linking of hydroxyethylcellulose in dilute aqueous solutions. J Phys Chem B. 2005;109(25):12329–36.
61. Bentz DP. Influence of water-to-cement ratio on hydration kinetics: simple models based on spatial considerations. Cem Concr Res. 2006;36(2):238–44.
62. Wadsö L, Winnefeld F, Riding K, Sandberg P. Calorimetry. In Scrivener K, Snellings R, Lothenbach B, (editors). A practical guide to microstructural analysis of cementitious materials. Boca Raton, FL: Taylor & Francis, 2016; p. 37–74.
63. Bentz DP. A review of early-age properties of cement-based materials. Cem Concr Res. 2008;38(2):196–204.
64. Bentz DP. Cement hydration: building bridges and dams at the microstructure level. Mater Struct. 2007;40(4):397–404.

65. Rattanasak U, Chindaprasirt P. Influence of NaOH solution on the synthesis of fly ash geopolymer. Miner Eng. 2009;22(12):1073–8.
66. Sashi P, Bhuyan AK. Viscosity dependence of some protein and enzyme reaction rates: seventy-five years after kramers. Biochemistry. 2015;54(29):4453–61.
67. Kumar A, Pawar SS. High viscosity of ionic liquids causes rate retardation of Diels-Alder reactions. Sci China-Chem. 2012;55(8):1633–7.
68. Pilehvar S, Szczotok AM, Rodríguez JF, Valentini L, Lanzón M, Pamies R, et al. Effect of freeze-thaw cycles on the mechanical behavior of geopolymer concrete and Portland cement concrete containing micro-encapsulated phase change materials. Constr Build Mater. 2019;200:94–103.

How to cite this article: Pilehvar S, Szczotok AM, Carmona M, Pamies R, Kjøniksen A-L. The effect of microencapsulated phase change materials on the rheology of geopolymer and Portland cement mortar. *J Am Ceram Soc*. 2020;00:1–18. https://doi.org/10.1111/jace.17215